CORONAGRAPHIC OBSERVATIONS AND ANALYSES OF THE ULTRAVIOLET SOLAR CORONA

NASA Grant NAG5-613

Annual Status Report Nos. 1 and 2

For the period 1 October 1994 to 30 September 1996

Principal Investigator
Dr. John L. Kohl

Prepared for
National Aeronautics and Space Administration
Wallops Island, VA 23337

Smithsonian Institution
Astrophysical Observatory
60 Garden St.
Cambridge, MA 02138 U.S.A.

The Smithsonian Astrophysical Observatory
is a member of the
Harvard-Smithsonian Center forAstrophysics

The NASA Technical Officer for this grant is Mr. Larry J. Early, Code 840.0, Goddard Space Flight Center/Wallops Flight Facility, Wallops Island, VA 23337.

UVCS/Spartan 201 Status Report

INTRODUCTION

This status report for the period 1 October 1994 to 31 July 1996 covers the postflight activities for the Spartan 201-2 mission and the preparations for and flight of the Spartan 201-3 mission. The analysis and publication of data from the first two flights and the postflight instrument characterization for Spartan 201-3 were also performed in this period. Results from the second and third flights confirm the presence of enhanced wings on the hydrogen velocity distributions and also confirm the Doppler dimming of the intensity of H I Lyman α in coronal holes which suggests the presence of high outflow velocities ($V > 150\ km\ s^{-1}$). The profile wings are most evident in the observed coronal holes. The results of the H I Lyman α profile measurements from the north and south coronal holes during the Spartan 201-1 flight were published in *The Astrophysical Journal.* (See list below.) The observations are consistent with a line of sight model that attributes the narrow component to background streamers and to sites within polar coronal holes or a surrounding diffuse corona and the broad component to the polar coronal holes and/or plumes. This interpretation suggests that there are regions within the observed coronal holes that have hydrogen and proton kinetic temperatures of $4 - 6 \times 10^6 K$ which is 4–10 times higher than the expected electron temperatures at the same heights. However, other models with, for example, local non-Maxwellian (Kappa) velocity distributions are also consistent with the observations. Further development of the line of sight model to include the Doppler dimming outflow velocity results is in progress.

List of Talks and Publications:

The following presentations and publications have been produced as a result of Spartan Missions 201-1 and 201-2.

- Cohen, C.M.S., Galvin, A.B., Gloeckler, G., Ko, Y-K., Strachan, L., Gardner, L.D., Kohl, J.L., Guhathakurta, M., Fisher, R.R., Geiss, J. and von Steiger, R. 1995 "Initial Results of a Collaboration between SWICS/Ulysses and Spartan 201 Observations of the Southern Polar Coronal Hole," *EOS, Trans. AGU, Suppl.* **76**, no. 17, 241.

- Kohl, J.L., Gardner, L. D., and Strachan, L. 1995, "UVCS/Spartan 201 Results for Proton Temperatures in the Extended Solar Corona," *EOS, Trans. AGU, Suppl.* **76** no. 46, 450.

- Kohl, J.L., Gardner, L.D. , Strachan, L., Fisher, R., and Guhathakurta, M. 1995, "Spartan 201 Coronal Spectroscopy During the Polar Passes of Ulysses", *Space Science Reviews* **72**, 29.

- Strachan, L., Gardner, L. D., and Kohl, J. L. 1995, "Recent Results from Spartan 201," presented at the UVCS/SOHO Science Meeting, Cambridge, (8-9 May 1995).

- Strachan, L., Gardner, L. D., and Kohl, J. L. 1995, "New Results for Outflow and LOS Velocities in the Solar Wind Acceleration Region of the Corona," *BAAS* **27(2)**, 970.

- Gardner, L.D., and Strachan, L., Smith, P.L., Kohl, J. L., and Lee, A. 1996, "Kinetic Temperatures and LOS Velocity Distributions in Polar Coronal Holes from UVCS/Spartan Observations", *EOS, Transactions, AGU, Suppl.* **77**, no. 17, 208.

- Kohl, J.L., Strachan, L., and Gardner, L.D. 1996, "Measurement of Hydrogen Velocity Distributions in the Extended Solar Corona", *Ap. J.* **465**, L141.

- Kohl, J.L., Gardner, L.D., and Strachan, L., Cohen, C.M.S., Galvin, A.B., Gloeckler, G., Guhathakurta, M., Fisher, R.R., Ko, Y-K., Geiss, J., von Steiger, R. 1996, "Proton Temperatures, Electron Temperatures and Outflows in the Extended Solar Corona" in *Ninth Cambridge Workshop on Cool Stars, Stellar Systems and the Sun*, eds. R. Pallavicini and A.K. Dupree, ASP Conference Series, (in press).

- Kohl, J.L, Gardner, L.D., Strachan, L., Noci, G., UVCS/Spartan 201 and UVCS/SOHO Teams 1996, "Measurements of H I and O VI Velocity Distributions in the Extended Solar Corona with Spartan 201 and UVCS/SOHO", presented at the 31st COSPAR Scientific Assembly, Birmingham, UK (14-21 July 1996).

- Strachan, L., Gardner, L. D., Smith, P.L., and Kohl, J. L., Guhathakurta, M., Fisher, R.R. 1996, "UVCS/Spartan Outflow Velocity Determinations in Polar Coronal Holes", *EOS, Transactions, AGU, Suppl.* **77**, no. 17, 208.

- Strachan, L., Gardner, L. D., Smith, P.L., and Kohl, J. L. 1996, "UV Spectroscopy of the Extended Solar Corona: Results from UVCS/Spartan", presented at the Workshop on the Scientific Basis for Robotic Exploration Close to the Sun, Marlboro, MA (15-18 April 1996).

- Strachan, L., Gardner, L. D., and Kohl, J. L. 1996, "Spatial distribution of Proton Temperatures and Outflow Velocities in a Coronal Streamer" (in preparation)

RESULTS FROM THE UVCS/SPARTAN 201-2 FLIGHT

Overview of UVCS/Spartan Observations

Four coronal targets were selected for observation during the Spartan 201-2 flight. The north and south coronal holes and two streamer regions were observed. The locations of

the UVCS spectrometer slits are for all of the coronal and disk observations are shown in Figure 1. The smallest slits are those used for making H I Lyα profile measurements, the intermediate slits are used for the O VI $\lambda\lambda$1032/1037 intensity measurements, and the largest slits are used for intensity measurements of H I Lyα and Fe XII λ1242.

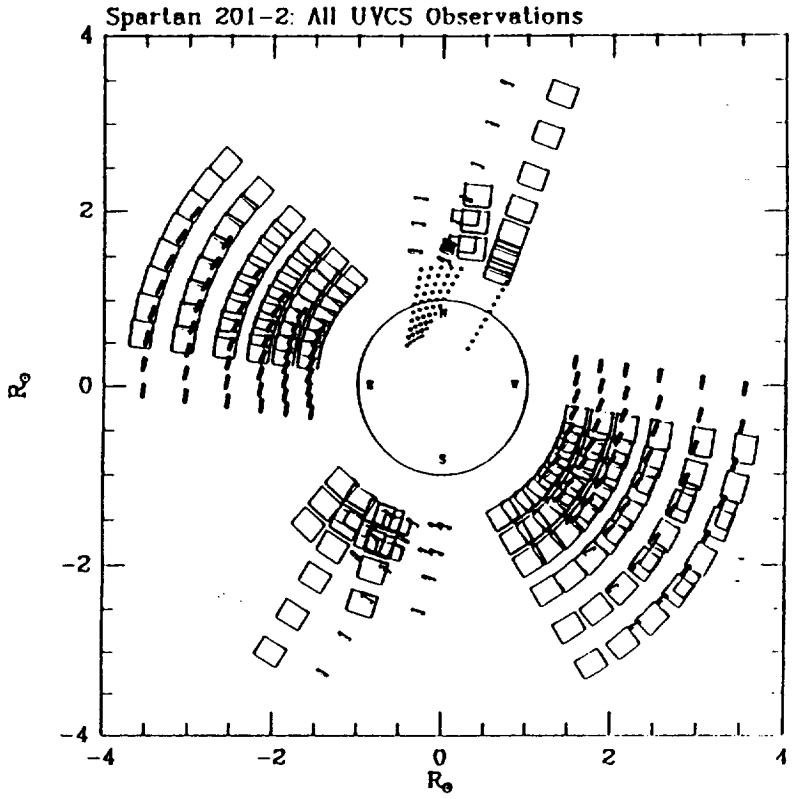

Figure 1: Spatial elements observed by the Ultraviolet Coronal Spectrometer during the Spartan 201-2 mission are illustrated. Normally, the UVCS instrument can observe three fields of view simultaneously. The smallest and largest rectangles are for observations of the line profile and integrated line intensity of H I Lyman alpha, and the intermediate sized rectangles are for the intensity of the O VI lines. (There are relatively fewer O VI observations because the O VI detector was not turned on for most of the flight.) Telescope motions are used to vary the heliocentric height and the entire spacecraft is rotated to vary the position angle. Small circles show the locations of H I Lyman alpha and O VI observations made with the disk mask.

The primary target was the south coronal hole which produced the fast solar wind streams that were being sampled by the Ulysses spacecraft at 80° heliographic latitude at 2 AU from the Sun. The Spartan observations in the south coronal hole were combined with data from the SWICS instrument on Ulysses to estimate outflow velocities by a Doppler dimming analysis of the H I Lyα intensities. These results are described below.

The north polar coronal hole was also observed along two position angles that covered the darkest regions of the corona, based on SXT/Yohkoh and Mauna Loa white light coronagraph pictures. By looking at both the north and south polar holes, data from one coronal hole can be compared with the other.

No distinct and clearly isolated helmet streamers were observed with the preflight planning data so the Lyα slits were placed on the regions of maximum brightness in the streamer belt. The Lyα observations covered active region streamers and possibly an equatorial coronal hole which was located near the west limb.

Disk observations were made near the north limb. There were five disk scans for the Lyα channel and one for the O VI channel. The disk observations are used to obtain the absolute disk irradiance which is an important parameter for the coronal models used for modeling the resonantly scattered coronal intensities.

Not shown in Figure 1 are the five geocoronal observations made at look angles of 95°, 110°, 140°, 150°, and 160° from the Sun. These observations were made to collect data useful in characterizing the geocoronal emission. Background observations were also made during Spartan's passage through the Earth's umbra.

Polar Coronal Hole Observations

The primary target for the 201-2 flight was the south polar coronal hole in order to make coordinated observations with the Ulysses spacecraft which was above the south solar pole. UVCS/Spartan made H I Lyα observations at $\rho = 1.5$, 1.8, 2.1, 2.5, 3.0, and 3.5 on a non-radial scan along the axis of the south coronal hole. Three other scans were made at position angles of $\pm 10°$ and 14° from the central scan. Observations were also made at two position angles in the north polar cornal hole which appeared to have less foreground and background features projected at the base of the coronal hole. Lyα profile measurements were made near the north coronal hole axis out to $\rho = 3.5$ and at 14° east of the primary axis. The OVI spectrometer slits and the slits for measuring the line integrated intensities for Lyα and Fe XII λ1242 are displaced from the slits used for the Lyα profile measurements as shown in Figure 1. The OVI observations are discussed below.

The most significant result from the 201-2 flight is the confirmation of the broad wings on the Lyα profiles. Figure 2 shows an example of profile from the south coronal hole. The observed profiles are a measure of the line of sight velocity distribution of neutral hydrogen (and protons) in the corona. The broad wings indicate that some of the protons have velocities that are much larger than the velocities associated with a one million degree plasma. In fact, the coronal profiles (after correction for the geocoronal absorption/emission feature) are best described by a fit consisting of two gaussians. In most cases the narrow component is fitted with a gaussian that has an 1/e half-width which is equivalent to a proton temperature which is less than one million degrees while the broad component is fitted with a gaussian that has an 1/e half-width which is equivalent to a proton temperature of greater than 3–4 million degrees.

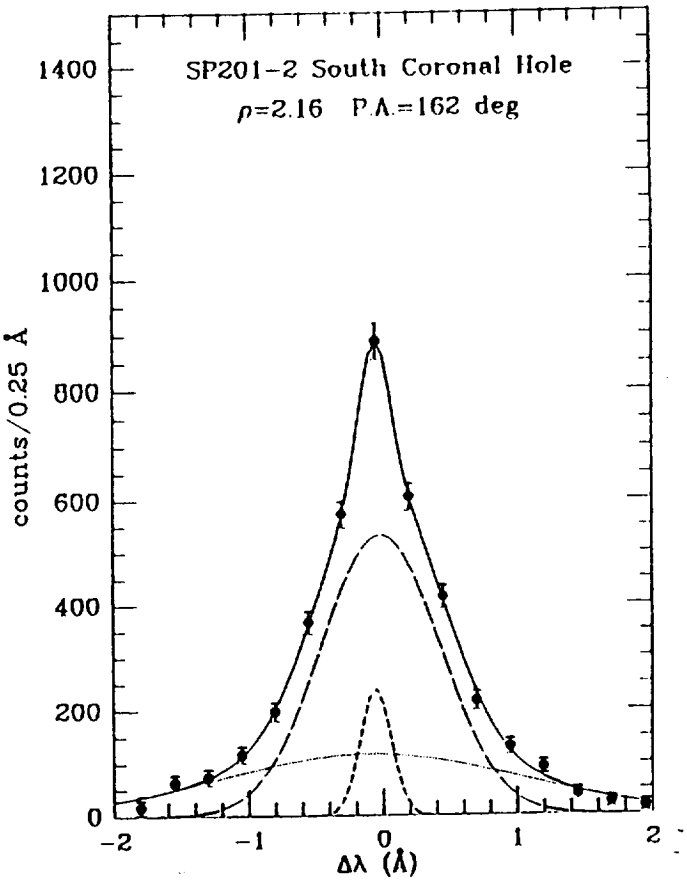

Figure 2: H I Lyman alpha profile from south coronal hole obtained at a heliocentric height of 2.16 $R_\odot$ and a position angle of 162 degrees. The profile has been fitted by three component gaussian curves. The narrowest component is due to the net geocoronal emission along the observed line of sight. The other two components make up the coronal Lyman alpha profile and have 1/e half-widths that correspond to kinetic temperatures of 1.4×10^6 K and 9.0×10^6 K. The most probable velocities corresponding to the widths are 152 km/s and 386 km/s.

There are several possible explanations for the observed Lyα line profiles (Kohl, *et al.* 1995). First the profiles could result from observing foreground or background structures in addition to the coronal hole along the same line of sight. Because of the different plasma conditions believed to exist in a foreground streamer, for example, and a coronal hole it is possible to have contributions from two very different line profiles along the same line of sight. In this scenario, UVCS/Spartan streamer observations suggest that the narrow profile component may be due to the streamer and the broad component would be coming from the coronal hole.

Another explanation is that coronal holes could be filled with mixed regions of different plasma conditions. The polar rays observed by the White Light Coronagraph during the first Spartan 201 flight give an example of a nonuniform corona with structures

that may fill the coronal hole along any individual line of sight.

A third possibility is that the complex profiles may show evidence of transverse MHD wave motions in coronal holes. The ratio of the areas for the two profile components would be an indication of the fraction of the line of sight affected by the waves.

It is also possible that the profiles are due to emission from a spatially uniform coronal hole with a non-Maxwellian proton velocity distribution. An example of this would be the kappa distributions proposed by Scudder (1992). These types of distributions result from high velocity particles that do not sufficiently thermalize as they rise from lower layers in the Sun.

Finally, the broad wings could be the result of non-radial bulk flows in the corona. The line of sight velocity components of the plasma will create red and blue-shifted components in the line profile. These and other explanations for the profiles are being studied by members of the UVCS/Spartan team and others in hopes of identifying the most likely cause for the observed effects.

Joint Science Results with SWICS/Ulysses

A collaboration has been established with the Solar Wind and Ion Composition (SWICS) Ulysses experiment group at the University of Maryland in order to combine thier freezing-in temperature measurements with the UVCS/Spartan Lyα data. Leonard Strachan has been working on this effort primarily with Christina Cohen (UMd). The SWICS freezing-in temperatures are calculated from ionization stages observed for different minor ions in the solar wind. The temperatures can be equated to the electron temperature (assuming local thermal equilibrium) at the coronal height where the ionization stage is 'frozen in'. We have then used the electron temperatures, thus derived, in a coronal hole model for the south polar hole. The electron temperatures are used in modelling the observed Lyα intensities.

Using electron temperatures derived from the SWICS/Ulysses data and electron densities derived from an extrapolation of white light data from the Mk III coronagraph at Mauna Loa, a Doppler dimming analysis of the Lyα intensities has been performed. Results show that average outflow speeds of 150 km/s are possible below $\rho = 3.5$ in the south coronal hole. Depending on the assumptions made about the neutral hydrogen scattering profile in the radial direction (which can't be observed directly), it is possible that even larger speeds exist.

Oxygen VI Observations

The number of O VI observations were limited for this flight since there was no vacuum pump operating to evacuate the detector. The concern was that, if the pressure inside the detector was too high, the detector would arc when high voltage is applied. To minimize the risk of arcing, the detector was not turned on until after spending the first 12 hours of the mission outgassing through the OVI detector entrance aperture.

Six orbits of coronal observations were made starting with the south coronal hole which was the second target of the mission. O VI observations were made at $\rho = 1.5$ and 1.8 for two position angles in the south coronal hole, at $\rho = 1.5$, 1.8, 2.1, 2.5, 3.0, and 3.5 for two position angles in the SW streamer region, and at $\rho = 1.5$ and 1.8 in the north coronal hole. There was also one scan across a portion of the solar disk. The only O VI "background" data was obtained during the five geocoronal observations which occurred when the satellite was in the Earth's umbra.

Significant progress was made in understanding some of the effects in the O VI data. It has now been demonstrated that the intensities for both O VI lines show a systematic variation with orbital position of the Spartan 201 spacecraft. Investigations of the effect for the first two flights show that it is more pronounced for the Spartan 201-2 observations which were obtained from a lower altitude (257 km vs. 294 km) than for the 201-1 observations. Leonard Strachan has been working on different atmospheric models to try to explain the atomic or molecular processes that may be responsible for these observations.

UVCS/SPARTAN FLIGHT 201-3

Characterization

Larry Gardner and Peter Smith completed optical alignment checks and the radiometric characterization of UVCS/Spartan as part of the Spartan 201-2 post-flight calibration and for the preparation for the Spartan 201-3 flight. The following measurements were performed on the Lyman-alpha spectrometer profile and intensity channels: 1) spectrometer entrance slit positions with respect to the critical occulter edge, 2) disk mask aperture position and throughput, 3) flat field measurements for both array detectors, 4) detector dark count rates, 5) cross-talk from one array detector to the other, 6) system radiometric calibration, and 7) wavelength setting. In addition, the vignetting function of the Lyman-alpha telescope mirror was measured.

Just after the 201-2 flight, the wavelength settings for the Lyα channel were checked and found to have held. Laboratory measurements of the Lyα channel required the diffraction grating to be moved, therefore, the Lyα wavelength position had to be re-established.

Larry Gardner successfully completed the change-out of the vacion pump on the Oxygen VI detector. The vacuum pump failed shortly before the Spartan 201-2 flight when it had reached the end of its useful lifetime. The decision was made to fly the mission with the nonoperating pump and to wait until after the UVCS/Spartan was de-integrated from the spacecraft before replacing the pump. The pump replacement was a difficult procedure because of the stringent requirement to limit the amount of time in which the OVI detector KBr photocathode coatings are exposed outside of vacuum.

After the new pump was installed, Larry Gardner and Peter Smith performed a radiometric characterization of the Oxygen VI channel. An atomic Nitrogen line at λ1039

was used for making a system radiometric calibration of the Oxygen VI 1037 channel. The Oxygen VI telescope mirror vignetting function was determined separately using the Ar I λ1048.

Reintegration of UVCS with the Spartan 201

The reintegration of the UVCS with the Spartan 201 spacecraft began in January 1995. Shortly after arrival at Goddard, the UVCS and WLC instruments were mated and installed into the Spartan Instrument Carrier which was assembled into the Service Module. Two 40-hour mission simulation tests occured in April 1995. UVCS/Spartan passed all tests with no major problems.

There were some problems with the spacecraft flight recorder during the first test which necessitated the need for a second 40 hour test. There were minor discrepancies in the flight recorder's performance but it was felt these were not serious.

In June, the spacecraft was shipped to KSC to begin the activities for integrating with the space shuttle. Other than a vacuum leak in the Spartan Instrument Carrier which was repaired, there were no major problems at KSC. A four-hour functional test proved that all mechanisms on the UVCS/Spartan instrument worked properly and the instrument was declared ready for flight.

Observing Program for Spartan 201-3

The UVCS/Spartan observing program was modified to optimize the coordinated science data to be obtained during the Ulysses north polar passage. The two coronal hole target sequences were both placed in the north coronal hole to give a more complete coverage of the hole spanning from its center to the eastern edge. The planned coronal observations are shown in Figure 3.

One orbit was removed from one of the streamer sequences in order to achieve the extended coronal hole coverage for this flight. With the new changes, both streamer target sequences were made to last for four orbits each. The changes do not affect the coverage for the streamers because they are much brighter than coronal holes and therefore they can be sampled with many more observations of shorter duration.

In order to characterize the source for the resonance scattering in the corona, observations are made on the disk of the Sun. In addition to the normal disk observation that was used for the previous Spartan 201 flights, a second observation was added which would observe the solar disk for the entire daylight portion of one orbit in order to characterize, as a function of orbital position and look angle, the daytime atmospheric layers that are above Spartan's orbit. This observation was planned near the end of the mission to minimize the risk of losing science data should a malfunction occur.

The number of geocoronal observations programmed for the mission was unchanged. These observations were made when Spartan is in the Earth's umbra with the UVCS instrument pointed 95°, 110°, 140°, 150°, and 160° away from the Sun.

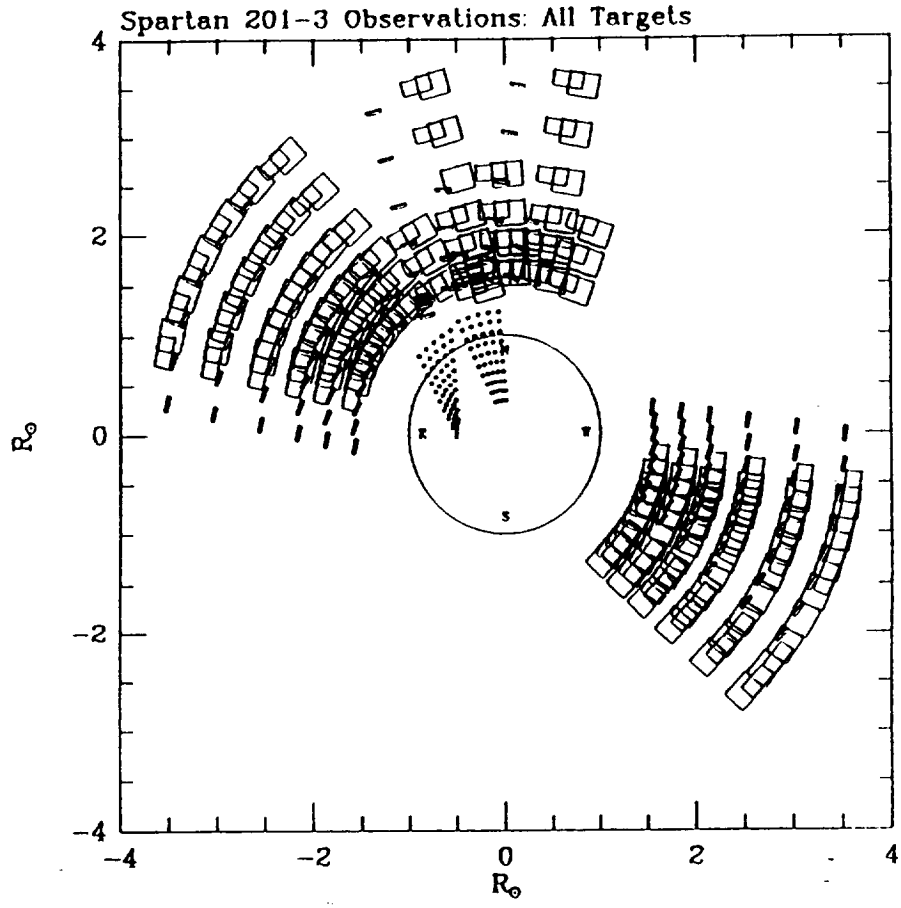

Figure 3: Spatial elements observed by the Ultraviolet Coronal Spectrometer during the Spartan 201-3 mission are illustrated.

Another modification concerns the operation of the Oxygen VI detector vacuum pump. Experience from the Spartan 201-2 flight showed that the Oxygen VI detector could be operated safely without the pump which is necessary to keep the detector evacuated when the instrument is on the ground. For the Spartan 201-3 flight, the pump was turned off in Orbit 6, after approximately 9 hours of pumping to reduce outgassing. Then the pump was programmed to turn on again at the end of Orbit 26.

Results from Spartan 201-3

The Spartan 201-3 mission ended prematurely when an End-of-Mission command was issued by the spacecraft. The early command resulted in a loss of the final two science orbits. The loss of the observations from Orbits 26 and 27 represented less than 10 percent of the entire planned observations. Missing are the second set of disk observations and a coronal hole observation at $\rho = 2.5$. The disk observation would have been useful in characterizing the effects from the terrestrial atmosphere above Spartan's orbit.

In the quick look analysis of Spartan 201-3 data, it was determined that the UVCS/Spartan instrument performed as expected. An inspection of the observations suggests broad wings on the observed Ly-alpha profiles in the north coronal hole as found in previous

flights. Ly-alpha profiles that were sampled from different coronal heights have count rates that are similar to those from the Spartan 201-2 flight, indicating no large change in system efficiency for the instrument. Also, background levels in the sample data set indicate that the detector performance and instrument stray light levels were normal. A check of an observation of the narrow geocoronal Ly-alpha line demonstrated that the spectrometer was in focus.

Detailed analyses of the data begun after the flight tapes were duplicated and distributed to the science teams. A new student, Alice Lee, provided part-time help in the extraction of the science data from the Spartan tapes and in the preliminary reduction of the Ly-alpha profiles. The first presentation of preliminary results from the 201-3 flight was given at the 1995 Fall AGU meeting.

Postflight Calibration for Spartan 201-3 and Refurbishment for Spartan 201-4

Post-flight alignment and co-registration checks at GSFC and at SAO showed no significant changes as a result of the STS-69 mission or of shipping from KSC to GSFC and from GSFC to SAO. One high voltage connector for the O VI pump was damaged during shipping; it has been replaced.

Functional tests at SAO showed that one of the detector accumulator boards had an intermittent fault that caused a null signal from every sixth pixel. This fault did not affect observations during 201-3. The flight board has been replaced with a spare, which will have to be qualified for 201-4. The problem with the bad board is being investigated.

All previous measurements of radiometric efficiency, detector flatfield and crosstalk, wavelength calibration, mirror vignetting function, and instrument profile for both channels of UVCS/Spartan have been made with the instrument cover removed. Because of the possibility that the telescope-spectrometer system may be distorted under these conditions, we are developing procedures for doing as many as possible of these characterizations before removing the cover. Fixturing for the new procedures has been produced and filters, photodiodes, and photomultipliers have been calibrated.

Lyα mirror vignetting function measurements showed there has been no significant loss of reflectivity at the edge of the mirror, which has received the maximum dose of damaging solar photons. The Lyα efficiency was found to be 0.37 percent. The spare telescope mirrors have been installed in a mirror holder and prepared for delivery to a vendor for coating.

Wavelength settings for the Lyα channel were checked and found to have held. The Lyα detector line profile is nominal at 1219 Å. (Measurements at the correct Lyα portion of the detector require removing the instrument cover.) Inter-detector crosstalk is nominal. Detector dark count rates are nominal.

THE ASTROPHYSICAL JOURNAL, 465:L141–L144, 1996 July 10

MEASUREMENT OF HYDROGEN VELOCITY DISTRIBUTIONS IN THE EXTENDED SOLAR CORONA

J. L. KOHL, L. STRACHAN, AND L. D. GARDNER
Harvard-Smithsonian Center for Astrophysics, Cambridge, MA 02138
Received 1996 March 8; accepted 1996 May 3

ABSTRACT

H I Lyα spectral line profiles have been measured in polar regions of the solar corona at projected heliocentric heights of 1.8–3.5 $R_\odot$. Observations were made with the Ultraviolet Coronal Spectrometer on the *Spartan 201* satellite from 16:52 to 04:04 UT on 1993 April 11–12 (south pole) and from 12:28 to 22:09 UT on 1993 April 12 (north pole). In general, the coronal profiles cannot be accurately curve-fitted with a single-Gaussian function. The fits with two Gaussians yield most probable velocities of 158 and 322 km s^{-1} (south) and 98 and 266 km s^{-1} (north). These parameters vary by less than 10% (1 σ) over the observed heights.

The observations are consistent with a line-of-sight model that attributes the narrow component to background streamers and to sites within polar coronal holes or a surrounding diffuse corona, and the broad component to the polar coronal holes and/or plumes. This interpretation suggests that there are regions within the observed coronal holes that have hydrogen and proton kinetic temperatures of (4–6) $\times$ 10^6 K, which is 4–10 times higher than the expected electron temperatures at the same heights. However, other models with, for example, local non-Maxwellian velocity distributions are also consistent with the observations.

Subject headings: solar wind — Sun: corona — Sun: UV radiation

1. INTRODUCTION

The spectral line profiles of H I Lyα in the extended solar corona provide a direct measurement of the velocity distribution of neutral hydrogen along the line of sight (LOS). Coronal H I Lyα is formed by resonant scattering of chromospheric H I Lyα by the small fraction of protons and electrons that exist as neutral H in the high-temperature corona (Gabriel 1971). For near 90° scattering, which tends to be the case for observations above the limb, the angular dependence of resonant scattering has only a small effect on the observed spectral line profiles (Withbroe et al. 1982). Hence, for precisions of ±10%, the observed line profile can be converted to a velocity distribution using the usual Doppler shift formula:

$$\frac{\Delta\lambda}{\lambda_0} = \frac{V}{c}, \qquad (1)$$

where $\Delta\lambda$ is the wavelength shift from the line center, λ_0, and c is the speed of light. Furthermore, the resulting H velocity distribution is believed to be representative of the coronal proton distribution (Withbroe et al. 1982; Leer 1988).

2. DESCRIPTION OF THE ULTRAVIOLET CORONAL SPECTROMETER/*SPARTAN 201* EXPERIMENT

The Spartan Ultraviolet Coronal Spectrometer is based on the design of a rocket instrument (Kohl, Reeves, & Kirkham 1978) and is described in Kohl, Gardner, & Strachan (1995). It is an externally and internally occulted reflecting telescope and a dual spectrometer. The telescope mirror used for H I Lyα has a 47.5 cm focal length and has an Al + MgF_2 coating. Mirror motions are used to scan radially from 1.5 to 3.5 $R_\odot$. An Ebert-Fastie spectrometer is used for H I Lyα. It has two entrance slits; one is 0.5 × 2.5 arcmin^2 to measure the line profile, and the other is 4.0 × 5.0 arcmin^2 to measure the total line intensity. The detector is a discrete anode microchannel array (Timothy, Mount, & Bybee 1981) with 48 pixels to measure the line profile with 0.25 Å spectral elements and 42 pixels to measure the line intensity with 2.0 Å spectral elements.

3. OBSERVATIONS

At the time of the observations, coronal holes at the north and south poles were dominant, long-lasting features in the corona. The electron densities and geometry of these structures, as determined by the Spartan White Light Coronagraph, have been described by Fisher & Guhathakurta (1995).

South polar region observations were made from 16:52 to 04:04 UT on 1993 April 11–12. In the following, we present profile measurements at several position angles starting at a projected heliocentric height (in $R_\odot$) of ρ = 1.83 and stepping out in height up to a maximum of ρ = 2.53. Four position angles separated by 10° and centered on the south coronal hole were observed. North polar region observations were made from 12:28 to 22:09 UT on 1993 April 12. Profile measurements were made along three position angles separated by 10°. An observation was also made in the north at ρ = 3.52.

Figure 1*c* shows the H I Lyα profile obtained at ρ = 3.52 in the north polar region. The data points show counts in each 0.25 Å resolution bin of the detector. The error bars indicate the ±1 σ uncertainties in the data (see § 4). A prominent feature of this profile is the narrow geocoronal component near the center of the profile. This feature is due to solar H I Lyα that undergoes resonant scattering by the neutral H in the atmospheric layers above *Spartan 201*'s orbit. The actual width of the geocoronal line is only 0.02 Å, but this is broadened by the instrument profile function. Figure 1*c* also demonstrates that the scattered light is negligible, since there is no component with the width of the chromospheric H I Lyα (Kohl et al. 1994).

Examples of other profiles from the north polar region are shown in Figures 1*a* and 1*b* and Figure 2*a*. In all cases the narrow geocoronal component has been removed. For comparison, a sample profile from the south polar region is shown

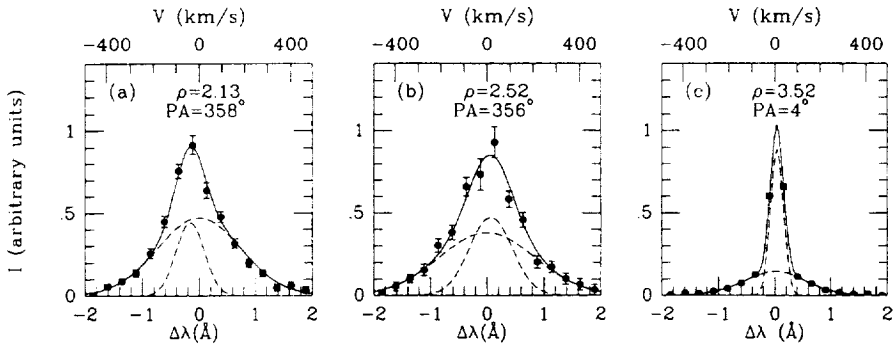

FIG. 1.—H I Lyα profiles from the north polar region showing 1 σ uncertainties in the data. Dashed curves in (*a*) and (*b*) are Gaussian components of the total coronal profile (*solid curve*). In (*c*) the two dashed components are the total coronal and net geocoronal contributions. The geocoronal contribution has been removed from the profiles in (*a*) and (*b*).

in Figure 2*b*. Both north and south profiles have extended wings with narrow profile cores.

4. DATA REDUCTION

The profiles in Figures 1 and 2 have been corrected for background counts and detector nonuniformities. The detector background was determined by averaging the pixel counts detected when *Spartan 201* was in the Earth's umbra and looking toward the Earth. A small exospheric contribution was subtracted from these measurements. The background correction is normally very small compared to the total counts in each pixel. After the background correction, the profile is corrected for detector cross-talk. This correction is based on laboratory measurements which have been shown to be constant during the time between the preflight and postflight calibrations. Approximately 2×10^{-3} of the peak counts in the intensity channel were subtracted from the counts in each pixel of the profile channel. The actual correction is different for each pixel. No artificial baseline correction has been made to force the wings of the profiles to go to zero. Nonetheless, the profile wings fall off to zero, which indicates that the detector backgrounds and corrections are well understood. Each profile also has been flat-field–corrected for the slightly different sensitivities of each pixel. This correction removes most of the unevenness in the distribution of the data, except for the irregularity that appears near the peak of some of the profiles.

5. PROFILE FITS

The profiles in Figures 1*a* and 1*b* and in Figures 2*a* and 2*b* are shown without the narrow geocoronal component. To remove this component, the observed profiles were fitted with three Gaussian curves, one of which was constrained to have the $1/e$ half-width of the instrument profile (0.16 Å). The wavelength position of that component, attributed to the geocorona, is known from Figure 1*c* and the known spacecraft velocity. This component accounts for both geocoronal emission and the absorption of coronal radiation by exospheric hydrogen.

Two Gaussians were used to fit the coronal profile, depending on goodness of fit. Goodness of fit was subjective but was determined by minimizing the χ^2 of the residuals at each data point. No constraints were made on the amplitude, width, or central-wavelength offset of the coronal Gaussians.

Figures 1 and 2 illustrate the curve fits for several representative profiles and also include the conversion of the wavelength scale to velocity using equation (1). We have used the streamer profile in Figure 2*c*, which has a single-Gaussian shape, to verify that the instrument profile cannot account for the enhanced line wings of the coronal hole profiles. Table 1 gives the parameters for these and other profiles observed in both polar coronal regions. I_{tot} is the total profile integrated intensity and I_B/I_{tot} is the ratio of the integrated intensity for the broad component to that of the total intensity. The most probable velocities, V_{mp}, for the narrow and broad profiles are in the columns labeled V_N and V_B. V_{mp} is the velocity where the profile (after being deconvolved from the instrument profile) is at $1/e$ of the maximum amplitude. The columns labeled ΔV_N and ΔV_B refer to equivalent velocity shifts of the profile components. All velocities have been corrected for the spacecraft orbital motion.

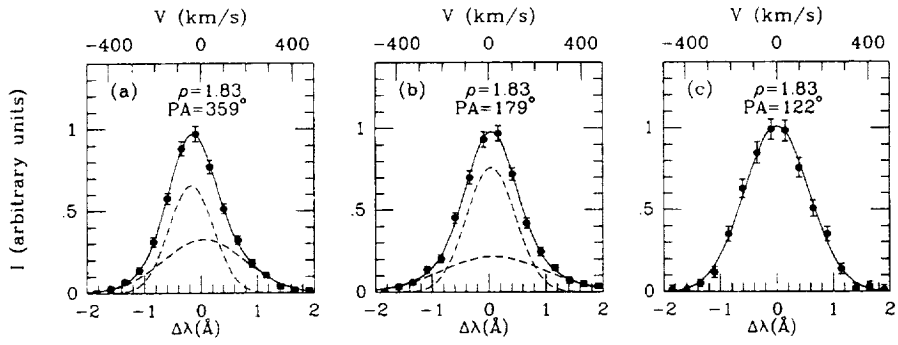

FIG. 2.—H I Lyα profiles from (*a*) the north polar region, (*b*) the south polar region, and (*c*) a helmet streamer. Dashed curves are Gaussian components to the total profile fit (*solid curve*). Note that the streamer profile data is fitted with a single Gaussian. The geocoronal contribution has been removed from all profiles.

TABLE 1

SPARTAN 201-1 H I Lyα PROFILE PARAMETERS

Height ($R_\odot$)	P.A. (deg)	I_{tot} (photons s^{-1} cm^{-2} sr^{-1})	I_B/I_{tot}	V_N (km s^{-1})	ΔV_N (km s^{-1})	V_B (km s^{-1})	ΔV_B (km s^{-1})
North Polar Region							
1.83.....	349.3	2.91×10^{10}	0.887	73	−36	196	−13
1.83.....	359.3	4.89×10^{10}	0.478	132	−41	250	14
1.83.....	9.3	3.99×10^{10}	0.459	130	−21	285	−6.6
Average	···	3.93×10^{10}	0.608	112	−33	244	−1.9
2.13.....	347.9	1.12×10^{10}	0.714	92	−23	327	−17
2.13.....	357.9	1.11×10^{10}	0.758	78	−44	255	−5
2.13.....	7.9	3.09×10^{10}	0.732	99	−20	223	−4.3
Average	···	1.77×10^{10}	0.735	90	−29	268	−8.8
2.52.....	346.5	2.29×10^{10}	0.832	75	−52	326	−9.6
2.52.....	356.5	7.27×10^{9}	0.642	125	11	292	−6.7
Average	···	1.51×10^{10}	0.737	100	−20	309	−8.2
3.52.....	4.3	1.65×10^{9}	0.653	92	−5.4	243	−13
South Polar Region							
1.73.....	189.9	4.34×10^{10}	0.336	147	0.3	330	12
1.83.....	179.3	2.39×10^{10}	0.375	144	10	312	20
1.83.....	189.3	2.46×10^{10}	0.231	163	4.5	353	−26
1.83.....	199.3	2.37×10^{10}	0.272	162	19	355	36
1.83.....	209.3	3.38×10^{10}	0.349	144	22	316	9.7
Average	···	2.65×10^{10}	0.307	153	14	334	9.9
2.13.....	177.9	6.93×10^{9}	0.416	188	25	511	30
2.13.....	187.9	7.04×10^{9}	0.516	169	18	275	−4.6
2.13.....	207.9	6.24×10^{9}	0.804	145	2.3	219	43
Average	···	6.74×10^{9}	0.579	167	15	335	23
2.52.....	186.5	1.93×10^{9}	0.525	170	−22	275	75
2.52.....	206.5	2.52×10^{9}	0.658	157	24	301	39
Average	···	2.23×10^{9}	0.592	164	1	288	57

6. DISCUSSION

It is clear that the velocity distribution along the LOS in the polar regions is not a single Gaussian as might be expected for an approximately isothermal LOS. Instead we find a coronal profile that is well fitted to two Gaussians after backgrounds and a geocoronal contribution are removed. If we average the V_{mp}'s for each component at each height, we find little variation with height. For the north polar region the narrow (broad) component has an average value of 98 km s^{-1} (266 km s^{-1}), corresponding to 5.8×10^5 K (4.3×10^6 K), and for the south polar region the narrow (broad) component has an average value of 158 km s^{-1} (322 km s^{-1}), corresponding to 1.51×10^6 K (6.28×10^6 K) for all observed heights.

The observed H I Lyα profiles suggest either a coronal plasma with sites along the LOS that have very different kinetic temperatures or a plasma with local non-Maxwellian velocity distributions. In the following, we discuss examples of each case and their consistency with the observations.

An example of the first case, discussed by Axford (1995), is that the LOSs through the polar corona have contributions from three sites: the tips of high-latitude helmet streamers, a diffuse corona adjacent to polar coronal holes, and the coronal holes themselves, including polar plumes. The contribution from streamers to the south polar region observations can be estimated from H I Lyα observations of a streamer that was above the southeast limb at position angle 131° at the time of the observations. This streamer appears to follow a neutral line that extends from Carrington longitude −180° to +30° (Real 1993). Observations with the Mark III coronagraph on Mauna Loa indicate that streamers at the approximate latitude of this streamer were present near the plane of the sky for at least a half-rotation before and after the *Spartan 201* observations. It appears that the streamer nearly encircles the Sun, and is shaped like an archway along the observed neutral line.

Spartan 201 white-light images (Fisher & Guhathakurta 1994) of the streamer indicate that it is not radial. A streamer archway with the observed orientation would be expected to intersect the LOS for the H I Lyα observation for $\rho = 1.83$ at about 3.5 $R_\odot$ in the background but not the foreground. The V_{mp} and intensity of the streamer at 3.5 $R_\odot$ were determined by the Spartan Ultraviolet Coronal Spectrometer (Strachan et al. 1994) to be $V_{mp} = 190$ km s^{-1} and $I = 8.6 \times 10^9$ photons s^{-1} cm^{-2} sr^{-1}.

The average value of V_{mp} for the narrow component in the south polar region at $\rho = 1.83$ is 153 km s^{-1}. The difference from the streamer value at 3.5 $R_\odot$ might be explained by another contribution to the narrow component, such as the coronal hole or a diffuse corona surrounding the coronal hole. It can be seen from Table 1 that the average intensity of the narrow component at $\rho = 1.83$ in the south is 1.84×10^{10} photons s^{-1} cm^{-2} sr^{-1}. This is approximately twice the inten-

sity of the streamer at the intersection point. The larger observed intensity is further evidence of another contributor to the narrow component.

In the case of the north polar region, there are no high-latitude streamers with intensities approaching that of the ones in the south. The fact that the broad component is a larger fraction of the total intensity in the north is consistent with the absence of bright streamers. The value of V_{mp} for the narrow component is significantly smaller than for the south hole at all observed heights.

As mentioned above, the narrow component of the two-Gaussian fits may be attributable to several sites. In at least the south polar region, streamers appear to contribute about half of the observed intensity, but have a larger line width than is observed. The remainder of the narrow component may have a width similar to that observed in the narrow component of the north polar region. It could be formed in the coronal hole itself or in the diffuse corona. We are left with the broad component being attributed to the coronal hole and/or plumes with a kinetic temperature of 4–10 times the expected electron temperature (Habbal, Esser, & Arndt 1993). Hence, the observations are consistent with mechanisms discussed by McKenzie, Banaszkiewicz, & Axford (1995) that preferentially heat particles in proportion to their mass.

It appears that explanations with a local non-Maxwellian velocity distribution do not account, at least, for the streamer contribution to the south hole. However, the coronal hole contribution could result from a combination of thermal velocities and transverse wave motions (Leer 1988). There also could be some contribution from nonradial outflows. Scudder (1992) has described mechanisms for producing non-Maxwellian distributions in low-density plasmas.

The velocity shifts in Table 1 suggest that the narrow and broad components correspond to different outflows and, therefore, have different origins. In the south polar region the narrow profile components show small LOS velocities which are not distinct from zero within the scatter of the data. The fact that the LOS velocities are small further supports the idea that the narrow component is due, in part, to the background streamer arcade, which is expected to have a low outflow velocity. (The small positive mean LOS values may be due to the fact that some of the intensity in the narrow component is due to material in the coronal hole itself.) The hot material in the south polar region (responsible for the broad profile) has LOS velocity components whose mean value increases steadily with height and, hence, appears to be associated with outflows from the coronal hole.

The hot sites in the north coronal hole have mean LOS velocity shifts that are small and negative but essentially zero. This implies that those hot sites have outflows with nearly equal amounts of material flowing forward and backward along the LOS. The large negative shifts of the narrow profile component may be due to cooler sites in the coronal hole that are moving toward the observer. This is consistent with the idea that some of the narrow component comes from sites in the coronal hole that contribute to the solar wind but are distinct from the sites that form the broad component.

The authors wish to thank D. Daugherty for assistance in reducing the flight profile data. This work was supported by NASA under grant NAG5-613 to the Smithsonian Astrophysical Observatory.

REFERENCES

Axford, W. I. 1995, private communication
Fisher, R. R., & Guhathakurta, M. 1994, Space Sci. Rev., 70, 267
———. 1995, ApJ, 447, L139
Gabriel, A. H. 1971, Sol. Phys., 21, 392
Habbal, S. R., Esser, R., & Arndt, M. B. 1993, ApJ, 413, 435
Kohl, J. L., Reeves, E. M., & Kirkham, B. 1978, in New Instrumentation for Space Astronomy, ed. K. A. van der Hucht & G. Vaiana (New York: Pergamon), 91
Kohl, J. L., Gardner, L. D., Strachan, L., & Hassler, D. M. 1994, Space Sci. Rev., 70, 253
Kohl, J. L., Gardner, L. D., & Strachan, L. 1995, Space Sci. Rev., 72, 29
Leer, E. 1988, in Proc. Sixth Int. Solar Wind Conf., ed. V. J. Pizzo, T. E. Holzer, & D. G. Sime (NCAR/TN-306+Proc.; Boulder: NCAR), 89
McKenzie, J. F., Banaszkiewicz, M., & Axford, W. I. 1995, A&A, 303, L45
Real, D. 1993, Prelim. Report Sol. Geophys. Data (SESC PRF 919; Boulder: NOAA-USAF/SESC), 22
Scudder, J. D. 1992, ApJ, 398, 319
Strachan, L., Gardner, L. D., Hassler, D. M., & Kohl, J. L. 1994, Space Sci. Rev., 70, 263
Timothy, J. G., Mount, G. H., & Bybee, R. L. 1981, IEEE Trans. Nucl. Sci., NS-28, 689
Withbroe, G. L., Kohl, J. L., Weiser, H., & Munro, R. H. 1982, Space Sci. Rev., 33, 17